第34卷 第2期 焊 接 学 报 Vol. 34 No. 2
2013年2月 TRANSACTIONS OF THE CHINA WELDING INSTITUTION February 2013

薄板铝合金高功率 CO_2 激光与光纤激光焊接飞溅特性对比分析

蔡 华，肖荣诗
（北京工业大学 激光工程研究院，北京 100124）

摘 要： 铝合金激光深熔焊接飞溅影响焊接稳定性并部分反映激光焊过程特性. 对比研究了 CO_2 及光纤激光焊接 6061-T6 铝合金的飞溅特性，探讨了两种激光焊飞溅特性差异的原因. 借助高速摄像仪记录飞溅运动特性，收集并测量焊接飞溅，采用 X^2 检验和最小二乘法拟合飞溅速度及尺寸分布. 结果表明，两种激光焊飞溅速度均服从高斯分布，飞溅尺寸均呈对数正态分布，但光纤激光焊飞溅统计平均速度更大，表明光纤激光焊时更需注重聚焦系统保护；光纤激光焊飞溅统计平均直径更小，拟合结果更服从对数正态分布，表明光纤激光焊过程比 CO_2 激光焊过程更稳定.

关键词： 薄板铝合金；高功率激光焊；飞溅特性；统计规律
中图分类号： TG456.7 **文献标识码：** A **文章编号：** 0253-360X(2013)02-0027-04

蔡 华

0 序 言

铝合金因轻质高强、抗耐蚀性好、易加工成形等优良性能，被广泛应用于航空、航天和汽车工业等领域. 但因铝合金热导率高、线膨胀系数大、传统热源发散、所焊铝合金构件变形大、晶粒粗大、力学性能较差[1,2]. 激光焊作为一种高能量密度、低热输入量、高柔性的先进连接方法，能实现高质量、低变形焊接结构[3,4]. 但激光深熔焊接铝合金时，由于激光束能量密度高，熔融态铝合金表面张力小，表面粘滞力小，材料蒸发强烈，引起焊接熔池及激光深熔小孔剧烈波动，产生大量飞溅.

铝合金深熔焊飞溅向熔池外迅速扩散，易污染聚焦反射镜，导致聚焦焦点位置变化、聚焦特性改变、焊接能量损失等问题，影响焊接质量[5]. 此外焊接飞溅的特性一定程度能反映激光焊过程的特性，如焊接熔池波动、焊接过程稳定性. Hyunsung 等人[6]采集镀锌钢 CO_2 激光焊飞溅的红外探测(IR)热辐射信号，飞溅 IR 信号随焊接过程波动而波动，IR 信号随焊接热输入量增加而增大. 激光焊工艺参数改变会影响焊接飞溅恶化焊接质量的程度，但目前对不同波长激光器与焊接飞溅的特性间的关系还未有研究报道. 文中通过设计试验，收集铝合金激光焊飞溅，观测焊接飞溅的实时运动特性、焊接飞溅尺寸及其形态，为减少焊接飞溅的污染聚焦系统提供数据依据，并着重对比了不同波长对激光焊飞溅特性的影响并探讨差异的形成原因.

收稿日期： 2011-12-05
基金项目： 国家自然科学基金资助项目(51175008)

1 试验方法

1.1 试验条件

采用德国 Rofin Sinar 公司 3 500 W Slab CO_2 激光器及 IPG 公司 YLS-6000 光纤激光器，聚焦镜焦距均为 300 mm，聚焦光斑直径分别为 0.26 mm 和 0.31 mm. 激光扫描焊接 2.0 mm 厚 6061-T6 铝合金，激光功率 $P=3$ kW，焊接速度 $v=4$ m/min.

采用 Photron Fastcam 高速摄像仪记录飞溅运动形态，如图 1 所示. 由于沿垂直焊件向上运动的飞溅物最易污染聚焦系统，试验布置高速摄像采集沿垂直焊件视场内的飞溅运动轨迹，测量为飞溅沿垂直焊件方向的速度分量 v_z.

图 2 为激光焊飞溅收集装置. 激光焊时，在与焊接运动方向平行，且距焊件 15 mm 处竖直放置捕捉板. 焊接工作头下方装置横向气帘，压缩空气通过气帘成为超音速气流，借助超音速气流迫使焊接飞溅附着于捕捉板，完成收集. 采用 PMG-3 金相软件观测收集的飞溅形态及尺寸.

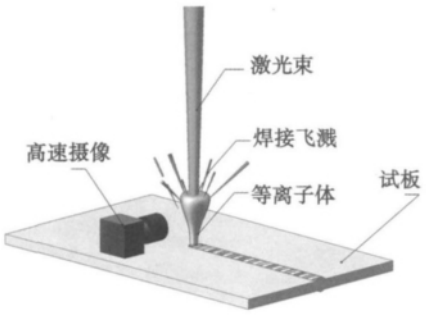

图 1 高速摄像观测焊接飞溅示意图

Fig. 1 High-speed observation for laser welding spatter

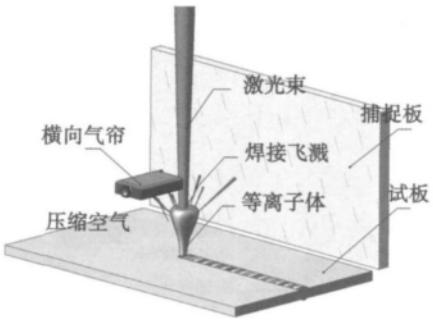

图 2 激光焊飞溅收集装置示意图

Fig. 2 Schematic for laser welding spatter collection

1.2 数据分析方法

利用 X^2 检验确定统计飞溅速度与尺寸的区间频率，得出样本频率分布；假设飞溅速度及尺寸理论分布，采用 Origin 软件最小二乘法迭代，拟合并检验假设理论分布；利用 95% 置信度下检验合格的理论分布比较 CO_2 激光焊和光纤激光焊飞溅特征.

根据最小二乘法理论，平均残差平方和(R_e) 越小则拟合分布越符合实际分布. 校正决定系数 R^2_{adj} 值越接近 1，则拟合优度越好.

2 试验结果

2.1 飞溅颗粒速度

图 3 为焊接飞溅高速摄像组图，CO_2 激光焊飞溅呈点状，光纤激光焊飞溅呈线状. 图 4 柱状图为 CO_2 激光焊及光纤激光焊飞溅运动速度分布及拟合曲线. CO_2 激光焊飞溅速度主要集中在 800 ~ 1 000 mm/s；光纤激光焊飞溅速度主要分布在 2 000 ~ 4 000 mm/s.

分析焊接飞溅速度分布(图 4) ，假设 CO_2 激光及光纤激光焊飞溅运动速度总体分布符合高斯分布，满足如下概率密度函数分布，即

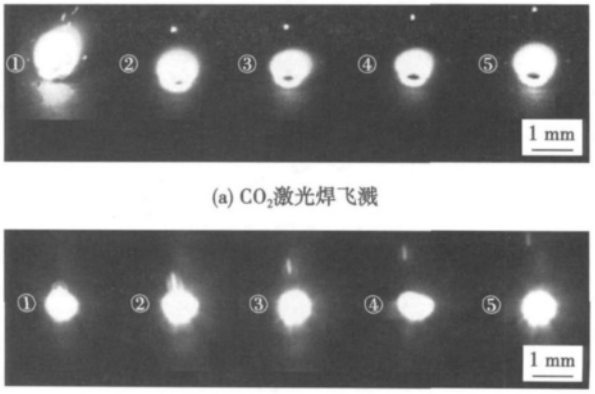

(a) CO_2激光焊飞溅

(b) 光纤激光焊飞溅

图 3 激光焊飞溅高速摄像图

Fig. 3 Video image of laser welding spatters

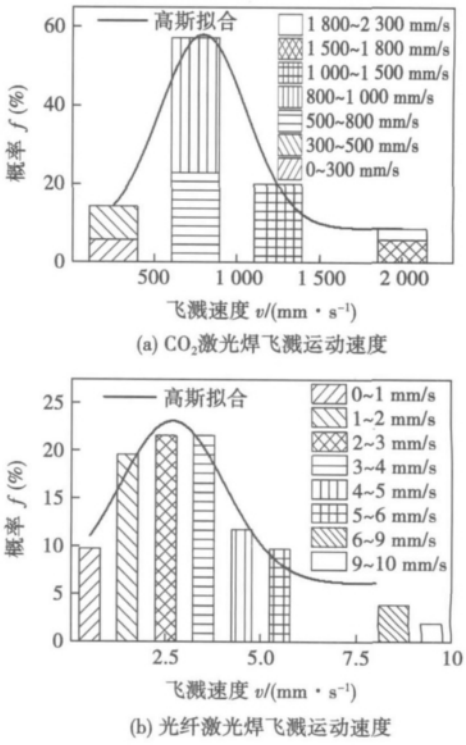

(a) CO_2激光焊飞溅运动速度

(b) 光纤激光焊飞溅运动速度

图 4 激光焊飞溅速度分布及拟合曲线

Fig. 4 Statistical chart of laser welding spatter in velocity

$$y = y_0 + \frac{A}{w\sqrt{\pi/2}} e^{-\frac{2(v_z - v_{zc})^2}{w^2}} \quad (1)$$

式中：y_0 为概率密度分布频率偏移；A 为曲线包围面积；w 为函数标准方差；v_z 为焊接飞溅运动速度的随机变量；v_{zc}为焊接飞溅平均运动速度.

CO_2 激光焊及光纤激光焊飞溅速度分布拟合如图 4 曲线所示. 由表 1 知，置信度 95% 下，两个样本拟合平均残差平方和均较小，R^2_{adj} 均接近 1，表明拟合优度好，95% 置信度下飞溅运动速度符合高斯分布，二者分布函数如下.

表 1　激光焊飞溅运动速度拟合评价参量

Table 1　Fitting eigenvalues of welding spatter in velocity

焊接方式	平均残差平方和 R_e	校正决定系数 R^2_{adj}	置信度 σ
CO_2 激光	$3.252\,58\times10^{-6}$	0.999 999	95%
光纤激光	0.345 67	0.995 053	95%

CO_2 激光焊飞溅运动速度拟合分布函数为

$$y=8.57+\frac{32\,687.4}{528.0\sqrt{\pi/2}}e^{-\frac{2(v_z-798.3)^2}{528.0^2}} \quad (2)$$

光纤激光焊飞溅运动速度拟合分布函数为

$$y=6.18+\frac{58\,555.3}{2\,759.0\sqrt{\pi/2}}e^{-\frac{2(v_z-2\,672.7)^2}{(2\,759.0)^2}} \quad (3)$$

由式(2)和式(3)以及高斯分布的特征值可知,CO_2 激光焊飞溅统计平均速度 $v_{zc}=798.3$ mm/s,光纤激光焊飞溅统计平均速度 $v_{zc}=2\,672.7$ mm/s,约为 CO_2 激光焊飞溅统计平均速度的 3 倍.

2.2　飞溅颗粒尺寸

图 5 为收集飞溅颗粒宏观形貌. 焊接飞溅近似球形. 图 6 为 CO_2 及光纤激光焊飞溅尺寸分布及拟合曲线. CO_2 激光焊飞溅直径主要分布在 20 ~ 200 μm; 光纤激光焊飞溅直径主要分布在 3 ~ 100 μm.

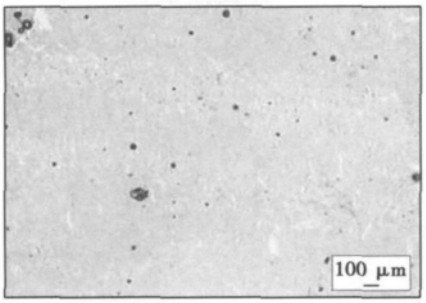

图 5　收集的焊接飞溅颗粒

Fig. 5　Photography of collected laser welding spatters

分析焊接飞溅尺寸分布(图 6),假设 CO_2 及光纤激光焊飞溅尺寸的总体分布符合对数正态分布,满足概率密度函数分布,即

$$y=y_0+\frac{A}{wx\sqrt{2\pi}}e^{-\frac{(\ln\phi-\ln\phi_c)^2}{2w^2}} \quad (4)$$

式中: ϕ 为焊接飞溅直径的随机变量; ϕ_c 为焊接飞溅平均直径.

CO_2 及光纤激光焊飞溅尺寸分布拟合曲线如图 6 所示. 由表 2 可知,置信度为 95% 时,两个样本拟合平均残差平方和都较小,R^2_{adj} 接近 1,表明拟合优度好,95% 置信度下,飞溅尺寸符合对数正态分布,二者分布函数如下. 此外从拟合质量及拟合优度上

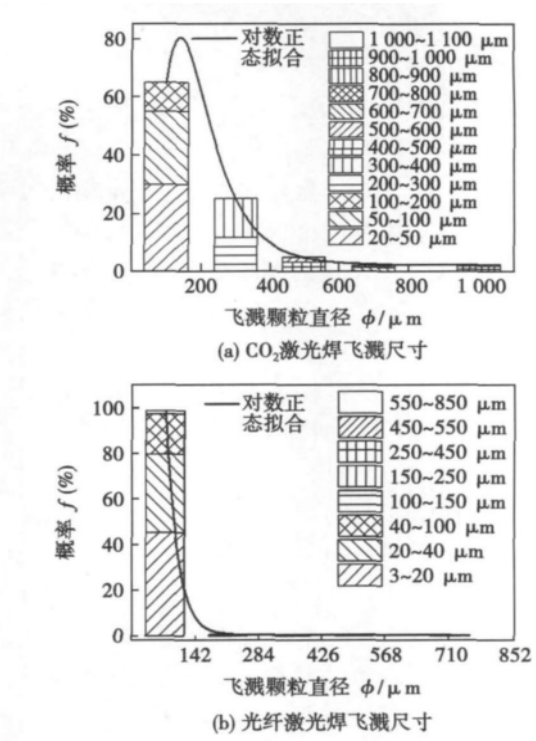

图 6　激光焊飞溅尺寸分布及拟合曲线

Fig. 6　Statistical chart of laser welding spatter in dimension

表 2　激光焊飞溅颗粒尺寸拟合评价参量

Table 2　Fitting eigenvalues of welding spatter in dimension

焊接方式	平均残差平方和 R_e	校正决定系数 R^2_{adj}	置信度 σ
CO_2 激光	0.109 39	0.999 850	95%
光纤激光	0.003 26	0.999 999	95%

说,光纤激光焊飞溅尺寸分布优于 CO_2 激光焊飞溅,表明光纤激光焊飞溅尺寸更符合对数正态分布.

CO_2 激光焊飞溅颗粒尺寸拟合分布函数为

$$y=2.36+\frac{15\,026.4}{0.49x\sqrt{2\pi}}e^{-\frac{(\ln\phi-\ln176.3)^2}{2(0.49)^2}} \quad (5)$$

光纤激光焊飞溅颗粒尺寸拟合分布函数为

$$y=0.17+\frac{10\,104.2}{0.45x\sqrt{2\pi}}e^{-\frac{(\ln\phi-\ln55.6)^2}{2\times0.45^2}} \quad (6)$$

由式(5)和式(6)以及对数正态分布特征值可知,CO_2 激光焊飞溅统计平均直径 $\phi_c=176.3$ μm,光纤激光焊飞溅统计平均直径 $\phi_c=55.6$ μm,约为 CO_2 激光焊飞溅统计平均直径的 1/3.

3　分析与讨论

CO_2 激光和光纤激光焊接飞溅尺寸均符合高斯分布,二者的焊接飞溅尺寸均符合对数正态分布,但

二者的飞溅运动速度和尺寸分布以及拟合评价参量均存在较大差异.

CO_2 激光器与光纤激光器波长相差较大(λ_{co_2} = 10.6 μm, λ_{fiber} = 1.07 μm) ,因此两种激光焊产生的等离子体差异很大. 激光焊过程中,金属蒸气对激光能量的吸收系数与激光波长平方成正比,故金属蒸气基本不吸收波长短的光纤激光能量,对其近似透明; 但易吸收长波长 CO_2 激光能量,导致金属蒸气温度升高,发生进一步热电离,并在极短时间内形成高温度、高密度金属等离子体[7,8]. 在 CO_2 激光焊过程中,只有较大尺寸的焊接飞溅才能够飞过高温度、高密度的金属等离子体而不被熔化或蒸发,故而 CO_2 激光焊飞溅颗粒的统计平均直径相对更大. 此外受等离子体波动的影响, CO_2 激光焊接熔池波动较大,焊接过程稳定性较差[9] ,且飞溅颗粒尺寸统计规律性相对较差. 光纤激光焊过程中仅产生温度及密度均相对较低的羽辉[10] ,从而较小尺寸的焊接飞溅也能够通过金属羽辉而不被熔化或蒸发,且由于羽辉波动相对等离子体波动很小,故光纤激光焊飞溅尺寸的拟合优度更好,规律性更强,焊接过程相对更稳定.

另一方面,铝合金材料更容易吸收波长较短的光纤激光器的能量[1] . 相比于 CO_2 激光焊,光纤激光焊过程中铝合金吸收更多的能量,飞溅颗粒运动速度相对更快. 从而由于光纤激光焊过程中飞溅颗粒运动速度过快,高速摄像视场有限,使得捕获飞溅运动形态不完全,造成速度数据样本误差,从而飞溅速度拟合优度相对较差. 此外焊接飞溅速度与飞溅尺寸密切相关,飞溅尺寸越小,质量越轻,在一定能量下,运动速度相对越快,即 CO_2 激光焊飞溅尺寸大于光纤激光焊飞溅尺寸,且 CO_2 激光焊飞溅运动速度小于光纤激光焊飞溅运动速度.

由试验及分析可知,光纤激光焊过程比 CO_2 激光焊接熔池波动小,焊接过程相对更加稳定. 同时,由于光纤激光焊飞溅运动速度相对更快,因此在光纤激光焊接时需要更注重聚焦镜的保护,防止飞溅污染. 而对于 CO_2 激光焊过程和光纤激光焊过程这两者的焊接特性差异需后续深入研究.

4 结 论

(1) CO_2 激光与光纤激光焊飞溅速度均服从高斯分布,焊接飞溅尺寸均符合对数正态分布.

(2) 光纤激光焊飞溅速度大于 CO_2 激光焊飞溅. 考虑到相对更快的飞溅运动速度,光纤激光焊接时需要更注重保护聚焦镜,防止飞溅污染.

(3) 光纤激光焊飞溅尺寸小于 CO_2 激光焊飞溅尺寸. 光纤激光焊飞溅尺寸统计规律性优于 CO_2 激光焊飞溅,反映了光纤激光焊接熔池波动小,焊接过程相对更加稳定.

(4) CO_2 激光焊与光纤激光焊飞溅特性差异较大,反映出 CO_2 激光焊与光纤激光焊过程差异较大.

参考文献:

[1] 左铁钏, 肖荣诗, 陈 铠, 等. 高强铝合金的激光加工[M]. 北京: 国防工业出版社, 2008.

[2] 崔 丽, 李晓延, 巩水利, 等. 5A90 铝锂合金激光焊焊缝微观组织特征[J]. 焊接学报, 2010, 31(9): 77 - 84.
Cui Li, Li Xiaoyan, Gong Shuili, *et al*. Microstructure investigation of Nd: YAG laser welded 5A90 aluminium-lithium alloys [J]. Transactions of the China welding Institution, 2010, 31(9): 77 - 84.

[3] Xiao R S. Laser beam welding of aluminum alloys [C] // Proceedings of SPIE-The International Society for Optical Engineering. Beijing, China, 2008: 1 - 10.

[4] 蔡 华, 肖荣诗, 陈 铠. 1420 铝锂合金 CO_2 激光焊接接头的力学性能研究[J]. 中国激光, 2009, 36(sl): 122 - 125.
Cai Hua, Xiao Rongshi, Chen Kai. Mechanical property of CO_2 laser welded joint of 1420 aluminum-lithium alloy [J]. Chinese Journal of Lasers, 2009, 36(sl): 122 - 125.

[5] Ribolla A, Damoulis G L, Batalha G F. The use of Nd: YAG laser weld for large scale volume assembly of automotive body in white [J]. Journal of Materials Processing Technology, 2005, 164: 1120 - 1127.

[6] Hyunsung P, Sehun R. Analysis of mechanism of plasma and spatter in CO_2 laser welding of galvanized steel [J]. Optics & Laser Technology, 1999, 31: 119 - 126.

[7] Zuo T C, Xiao R S, Volz R. Experimental research on the influence of laser-induced plasma on the beam focusing during high-power CO_2 laser materials processing [C] // Proceedings of SPIE-The International Society for Optical Engineering California, USA, 1998: 62 - 69.

[8] 祁俊峰, 丁 鹏, 张冬云, 等. 工艺参数对铝合金 CO_2 激光焊接光致等离子体温度的影响[J]. 焊接学报, 2008, 29(6): 97 - 100.
Qi Junfeng, Ding Peng, Zhang Dongyun, *et al*. Influence of welding parameters on laser-induced plasma temperature in CO_2 laser welding of aluminum alloys [J]. Transactions of the China welding Institution, 2008, 29(6): 97 - 100.

[9] 陈 铠, 肖荣诗, 张盛海, 等. 高强铝合金激光粉末焊接过程[J]. 焊接学报, 2006, 27(10): 33 - 36.
Chen Kai, Xiao Rongshi, Zhang Shenghai, *et al*. CO_2 laser welding process of aluminum alloy with filler powder [J]. Transactions of the China welding Institution, 2006, 27(10): 33 - 36.

[10] Kawahito Y, Matsumoto N, Katayama S, *et al*. Characterization of plasma induced during high power fiber laser welding of stainless steel [J]. Science and Technology of Welding and Joining, 2008, 13(8): 744 - 748.

作者简介: 蔡 华,女,1986 年出生,博士研究生. 主要从事铝合金激光加工及铝合金激光焊接头组织及性能分析方面的研究工作. 发表论文 1 篇. Email: shuangyaqing@emails.bjut.edu.cn

通讯作者: 肖荣诗,男,教授,博士研究生导师. Email: rsxiao@bjut.edu.cn

compounds started to react with Cu ball bonds to form Cu_3Sb. When the aging time is more than 49 hours at 250 ℃, Cu wire loop is broken and serious corrosion is found in Cu ball bond. Furthermore, Ag migration phenomenon occurs if the aging time is more than 24 hours at 250 ℃ or 4 hours at 300 ℃.

Key words: fine Cu wire; high temperature storage; IMC; reability; Ag migration

An ultrasonic SH-guided-wave transducer for ultrasonic imaging and testing of plate with welded structure ZHU Xinjie, CHEN Yifang, HAN Zandong, DU Dong (Key Laboratory for Advanced Materials Processing Technology, Ministry of Education, Tsinghua University, Beijing 100084, China). pp 17 – 21

Abstract: The SH (shear horizontal) guided waves can be used to test and image in long distance for the larger-sized plate in welded structure. The performance of ultrasonic SH-guided-waves transducer is essential to imaging and testing larger-sized plate in welded structure. The dynamic analysis of SH guided wave in plate and half-wave propagation conditions was carried out. The reasonable wedge angle, the frequency, size of the piezoelectric wafer for SH-guided-waves transducer and other important parameters were designed. The steps such as adding the front lining, removing the back lining, setting the jagged slot on front wedge and so on, have reduced the internal echo interference in SH-guided-waves transducer, which improves the testing sensitivity and simplifies the transducer structure. The results shows that the developed SH-guided-waves transducer has the better testing ability and can be used in imaging and testing complex T-butt type welded structure. The image can characterize the defects, whose size is close to the guided wave length in the welded structure. The proposed research provides the foundation for the imaging and testing of larger-sized plate with welded structure.

Key words: ultrasonic; shear horizontal-guided-wave transducer; welded structure

Effect rule of torch angle change on weld formation of keyhole plasma arc welding JIANG Fan, CHEN Shujun, WANG Long, YU Yang (College of Mechanical Engineering and Applied Electronics Technology, Beijing University of Technology, Beijing 100124, China). pp 22 – 26

Abstract: By taking 5 mm thick 5A06 aluminum-magnesium alloy as the main researching object, the front and back weld width as the formation parameter, the significance of torch angle to weld formation was studied by the orthogonal experiment, the effect of change of torch angle on weld formation was studied from the point of energy transfer. The result shows that the influence of the torch angle on welding formation is between current and plasma gas flow rate. There is largest front weld width when the torch is perpendicular to the test plate. The back weld width will be larger with the torch angle increasing. It indicates the energy density on the front surface, the relative position of the highest temperature section and the widest molten section will be changed by torch angle change. The effect on the back weld width may be caused by the interaction of sectional heat source deviation of different thickness direction and the delay of heat transfer.

Key words: keyhole plasma arc welding; torch travelling angle; weld formation; orthogonal experiment

Statistic analysis on spatter characteristics in high power CO_2 laser and fiber laser welding of thin sheet aluminum alloy CAI Hua, XIAO Rongshi (Institute of Laser Engineering, Beijing University of Technology, Beijing 100124, China). pp 27 – 30

Abstract: Spatters in laser penetration welding of aluminum alloys affects the process stability and reflects the laser welding process to a certain degree. The spatter characteristics in CO_2 laser and fiber welding of 6061-T6 aluminum alloy were investigated, and the reasons for the difference in spatter characteristics were discussed. Dynamic behavior of spatters was recorded in real-time by a high-speed camera. The spatter particles were captured and their sizes were measured experimentally. Probability density functions (PDFs) about the spatter velocity and size were fitted by Ordinary Least Squares (OLS) method in X^2 test. The result indicates that the spatter speed follows Gaussian distribution and the particle size follows lognormal distribution in both cases. However, the statistical speed of spatters is faster in fiber laser welding, which indicates that more attention should be paid to protect the focusing system. Moreover, the statistical diameters of the spatter particles are smaller and PDFs of the particle size is more fit with Lognormal distribution in fiber laser welding, which means that fiber laser welding process is more stable than CO_2 laser welding process.

Key words: thin sheet aluminum alloy; high power laser welding; spatter characterization; statistic analysis

Selection method of X-ray diffraction stress measurement parameters for titanium and titanium alloy DENG Yunhua, LI Xiaoyan, LI Qingqing, LU Wei (School of Materials Science and Engineering, Beijing University of Technology, Beijing 100124, China). pp 31 – 34, 39

Abstract: Considering the low intensity of diffraction peak, bad diffraction profile, wide fluctuation range and low accuracy of the stress measurement results for titanium and titanium alloy, the effects of aperture diameter, exposure time, and exposure number on the intensity of X-ray diffraction peak, net intensity, full width at half maximum, and the stress measurement results were investigated through the X-ray stress measurement of free stress standard sample and high stress standard sample. On this basis, the selection method of X-ray diffraction stress measurement parameters for titanium and titanium alloy was decided and used in measuring the residual stresses in TC4 welded joint. Results show that with the increase of aperture diameter and exposure time, the intensity of X-ray diffraction peak increases, both the diffraction profile and the accuracy of the test results are improved. What's more, with the increase of exposure number, the diffraction profile and the accuracy of the test results are also improved. The measurement results of residual stresses in TC4 welded joint meet the requirements of the related standards.

Key words: titanium alloy; X-ray stress measurement;